# Electronic Supplementary Information (ESI)

## Design of Self-Righting Steam Generators for Solar-Driven Interfacial Evaporation and Self-Powered Water Wave Detection

Guoliang Chen, Na Li, Jintao He, Lifang Qiao, Fangbin Li, Shuxue Wang, Liangmin Yu, Petri Murto,* Xiaoyi Li* & Xiaofeng Xu*

* Corresponding authors: X. Xu, email: xuxiaofeng@ouc.edu.cn

X. Li, email: lixiaoyi@ouc.edu.cn

P. Murto, email: pm707@cam.ac.uk

## Table of Contents

## 1. Materials

Polyacrylonitrile (PAN, average $M_w$ = 150,000) was purchased by Mreda technology Inc., China. CB nanoparticles (average diameter: ~30 nm) were purchased from Shanghai Macklin Biochemical, China. Polyurethane (PU) prepolymer was purchased from Sinopharm Chemical Reagent Co., Ltd, China.

## 2. Materials characterization

The microstructures and morphologies of PAN aerogels, PAN/CB aerogels and PU foam were characterized by scanning electron microscopy (Phenom pro, Phenom Scientific) with an accelerating voltage of 10 kV. Contact angles were measured via a contact angle goniometer (JC2000DM, Powereach) by using 4 μL of water droplet as an indicator. The ATR−FTIR spectra were recorded via a Nicolet FTIR Infrared Microscope (iS50 FT-IR, Thermo Fisher Scientific). The reflectance spectra were measured via a UV−Vis−NIR spectrometer (Lambda 950, PerkinElmer) equipped with an integrating sphere. The density and porosity of samples were measured and calculated by a high-precision foam density tester (AU-120PF, Quarrz, accuracy: 0.1 mg cm$^{-3}$). The compression tests were performed using a universal mechanical testing system equipped a 100 N digital force gauges (M5-100, Mark-10, accuracy: 0.02 N) and a force test stand (ESM 303, Mark-10), at a strain rate of 2 mm min$^{-1}$ for stress−strain (σ−ε) tests; all samples were compressed up to 80% strain of their initial total length at ambient temperature. The Young's modulus was determined by the slope of the initial linear region of the stress-strain curve. The thermal conductivity of PAN aerogels and PU foam was measured by a homemade thermal conductivity testing system.
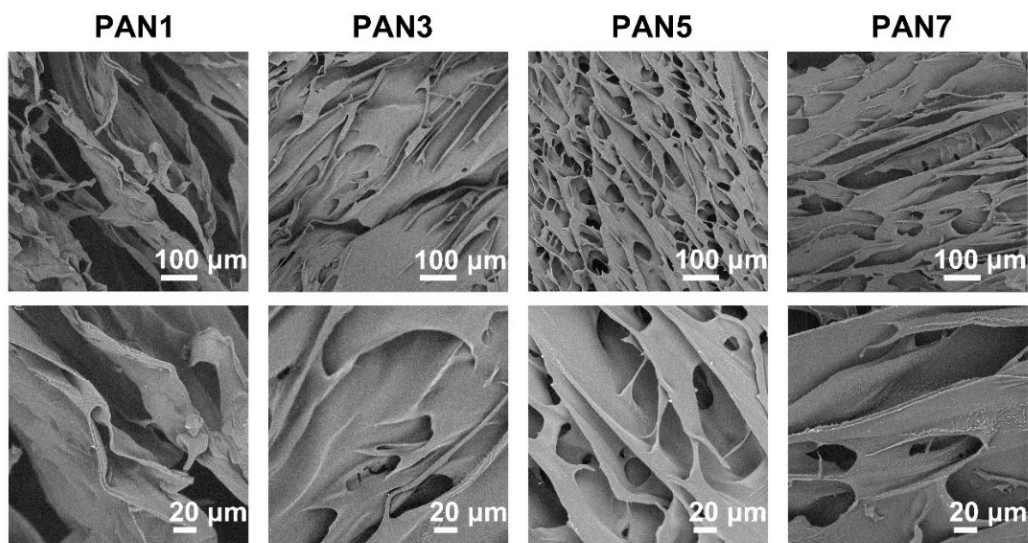
## 3. Scanning electron microscope (SEM) images



**Figure S1.** Cross-section SEM images of aerogels PAN1, PAN3, PAN5 and PAN7.
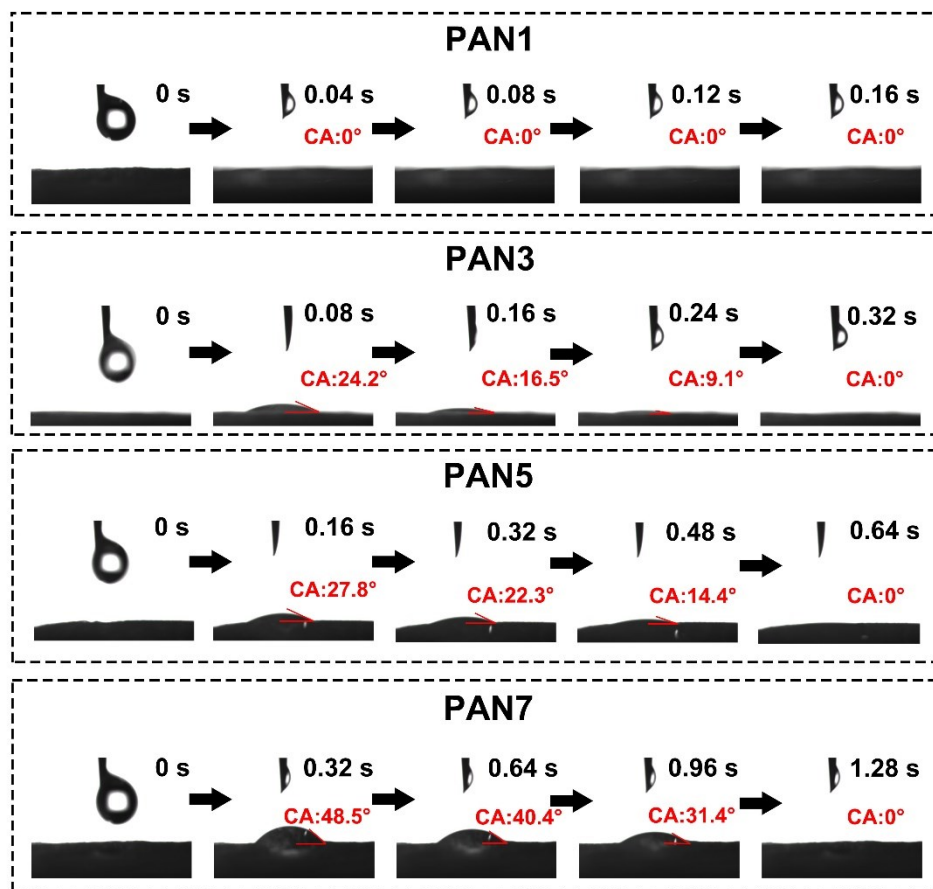
## 4. Water contact angle measurements



**Figure S2.** Digital photographs of dynamic contact angle measurements.
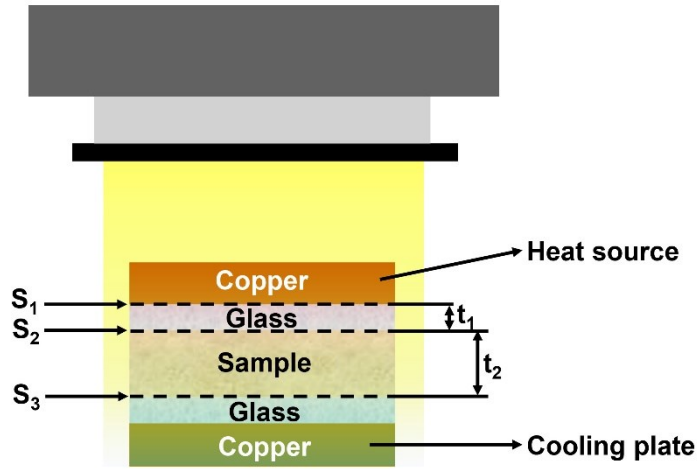
## 5. Thermal conductivity measurements



**Figure S3.** A schematic diagram of thermal conductivity measurements.

In the thermal conductivity tests, we used a xenon lamp to warm the samples. As shown in Figure S3, the sample to be tested was sandwiched between glasses and copper plates, and the upper copper plate was used as the heat source. The heat was successively transferred to the top glass, the sample, the lower glass and the lowest copper plate (cooling end). It was regarded to be in thermal equilibrium when the temperature fluctuation was less than 0.2 °C.

The thermal conductivity of samples can be calculated according to the following equation[1-3]: $q'' = k dT/dx$, where $q''$ is the heat flux, $dT/dx$ represents the temperature gradient of the cross-section in the vertical direction. So when the test system was in a thermally stable state, $k_g dT_1/dt_1 = k_s dT_2/dt_2$ was satisfied, where $k_g$ (1.05 W m$^{-1}$K$^{-1}$) and $k_s$ are the thermal conductivity of the glass and the sample, $dT_1$ and $dT_2$ are the temperature difference between interface S$_1$ and interface S$_2$ and the temperature difference between interface S$_2$ and interface S$_3$, $dt_1$ and $dt_2$ are the thickness of glass and samples, respectively.
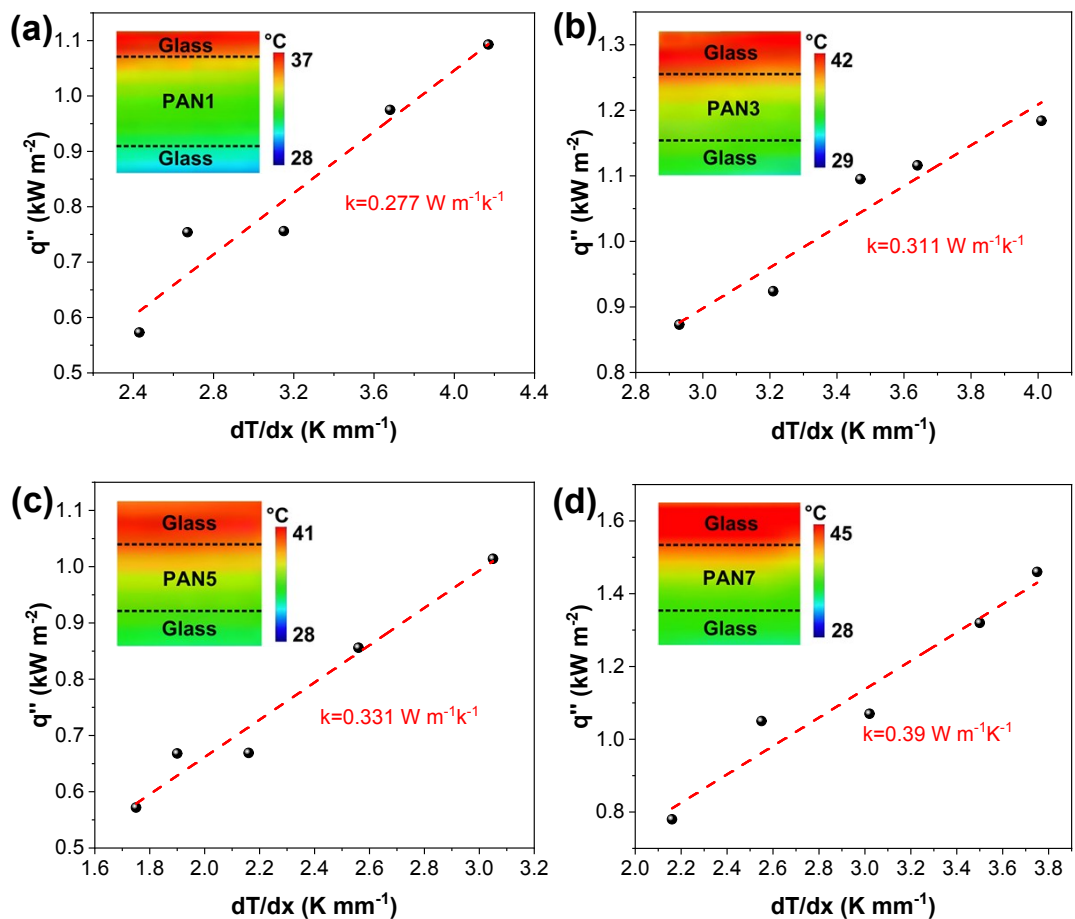
**Figure S4.** Thermal conductivity of PAN aerogels. (a) PAN1, (b) PAN3, (c) PAN5 and (d) PAN7.
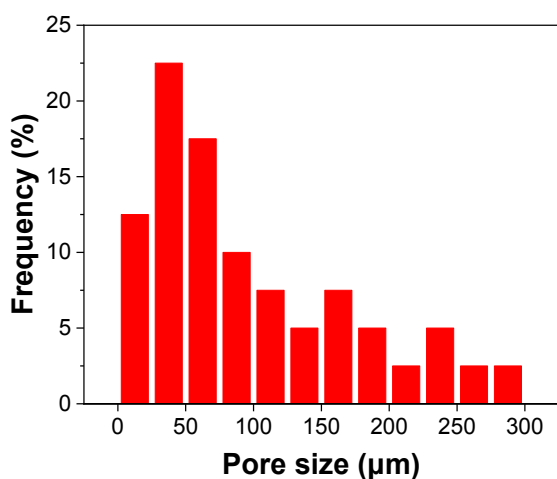
## 6. Pore size distribution of a PU foam



**Figure S5.** Pore size distribution of a PU foam.

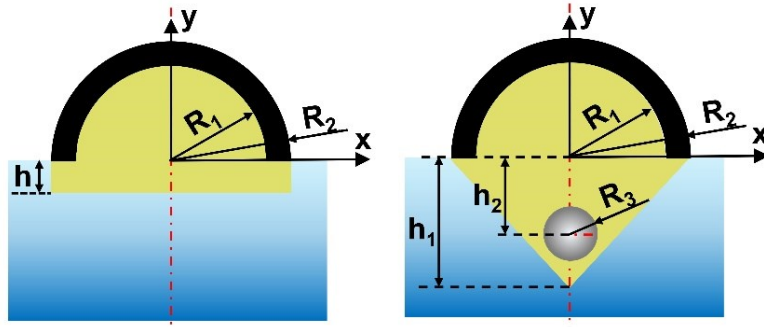# 7. Calculation of the center of gravity height



**Figure S6.** Schematics of a hemispheric steam generator (left) and a tumbler-shaped steam generator (right).

## (a) A hemispheric interfacial steam generator

According to Equation (2), the height of PU foam $h$ below the PAN/CB aerogel was

$$\frac{2}{3}\frac{\rho_w\left(R_2^{\,3}-R_1^{\,3}\right)+\rho_{pu}R_1^{\,3}}{R_2^{\,2}\left(\rho_w-\rho_{pu}\right)}$$. After calculated, the value of $h$ was 7.2 mm.

Firstly, the mass of wet PAN/CB aerogel $m_1$ (assuming that its density is the same as the density of water $\rho_w$) and its static moment on the x axis $m_1y_1$ are $\frac{2}{3}\rho_w\pi(R_2^{\,3}-R_1^{\,3})$ and

$\frac{1}{4}\rho_w\pi(R_2^{\,4}-R_1^{\,4})$, respectively. Secondly, the mass of the PU foam (its density is $\rho_{pu}$) above the water surface $m_2$ and its static moment on the x axis $m_2y_2$ are $\frac{2}{3}\rho_{pu}\pi R_1^{\,3}$ and $\frac{1}{4}\rho_{pu}\pi R_1^{\,4}$, respectively. The last, the mass of the PU foam below the water surface $m_3$ and its static moment on the x axis $m_3y_3$ are $\rho_{pu}\pi R_2^{\,2}h$ and $-\frac{h}{2}\rho_{pu}\pi R_2^{\,2}h$.

The height of center of gravity $Y_{G1}$ is calculated according to the following equation:

$$Y_{G1} = \frac{\sum\limits_{i=1}^{3} m_i y_i}{\sum\limits_{i=1}^{3} m_i} = \frac{3}{8} \frac{\rho_w \left(R_2^4 - R_1^4\right) + \rho_{pu} R_1^4 - 2\rho_{pu} R_2^2 h^2}{\rho_w \left(R_2^3 - R_1^3\right) + \rho_{pu} R_1^3 + \frac{3}{2}\rho_{pu} R_2^2 h}$$

$$= \frac{3}{8} \frac{\left(20^4 - 16^4\right) + 0.05 \times 20^4 - 2 \times 0.05 \times 20^2 \times 7.2^2}{\left(20^3 - 16^3\right) + 0.05 \times 20^3 + 1.5 \times 0.05 \times 20^2 \times 7.2} = 8.3 \ mm$$

**(b) A tumbler-shaped interfacial steam generator**

According to Equation (2), the mass $m_3$ of stainless-steel ball was calculated as

$$\frac{4}{3}\rho_s \pi \frac{\left(\rho_w - \rho_{pu}\right)R_2^2 h_1 - 2\rho_w \left(R_2^3 - R_1^3\right) - 2\rho_{pu} R_1^3}{4\rho_s - 3\rho_{pu}}$$ . After calculated, the value of $m_3$ was 4.15

g, we used a slightly heavier steel ball with a mass of 4.17 g.

First, the mass of PAN/CB aerogel $m_1$ and its static moment on the $x$ axis $m_1 y_1$ are

$\frac{2}{3}\rho_w \pi (R_2^3 - R_1^3)$ and $\frac{1}{4}\rho_w \pi (R_2^4 - R_1^4)$, respectively. Secondly, the mass of the PU foam

above the water surface $m_2$ and its static moment on the $x$ axis $m_2 y_2$ are $\frac{2}{3}\rho_{pu} \pi R_1^3$ and

$\frac{1}{4}\rho_{pu}\pi R_1^4$, respectively. Thirdly, the mass of the PU foam under the water surface $m_3$ and its

static moment on the $x$ axis $m_3 y_3$ are $\frac{1}{3}\rho_{pu}\pi R_2^2 h_1 - \frac{4}{3}\rho_{pu}\pi R_3^3$ and

$-\frac{1}{12}\rho_{pu}\pi R_2^2 h_1^2 + \frac{4}{3}\rho_{pu}\pi R_3^3 h_2$ ($h_2 \sim 20$ mm), respectively. The last, the mass of counterweight

(steel ball, its density $\rho_s$: 7.98 g cm$^{-3}$) below the water surface $m_4$ and its static moment on the

x axis $m_4 y_4$ are $\frac{4}{3}\rho_s \pi R_3^3$ and $-\frac{4}{3}\rho_s \pi R_3^3 h_2$, respectively.

The height of center of gravity $Y_{G2}$ was calculated according to the following equation:

$$Y_{G2} = \frac{\sum\limits_{i=1}^{4} m_i y_i}{\sum\limits_{i=1}^{4} m_i} = \frac{\frac{1}{4}\rho_w\left(R_2^4 - R_1^4\right) + \frac{1}{4}\rho_{pu}R_1^4 - \frac{1}{12}\rho_{pu}R_2^2 h_1^2 + \frac{4}{3}R_3^3 h_2\left(\rho_{pu} - \rho_s\right)}{\frac{2}{3}\rho_w\left(R_2^3 - R_1^3\right) + \frac{2}{3}\rho_{pu}R_1^3 + \frac{1}{3}\rho_{pu}R_2^2 h_1 + \frac{4}{3}R_3^3\left(\rho_s - \rho_{pu}\right)}$$

$$= \frac{\frac{1}{4}\left(20^4 - 16^4\right) + \frac{1}{4}0.05 \times 16^4 - \frac{1}{12}0.05 \times 20^2 \times 32^2 + \frac{4}{3}\times 5^3 \times 20\left(0.05 - 7.98\right)}{\frac{2}{3}\left(20^3 - 16^3\right) + \frac{2}{3}0.05 \times 16^3 + \frac{1}{3}0.05 \times 20^2 \times 32 + \frac{4}{3}5^3\left(7.98 - 0.05\right)} = -0.8 \ mm$$

## 8. A schematic diagram of water evaporation setup
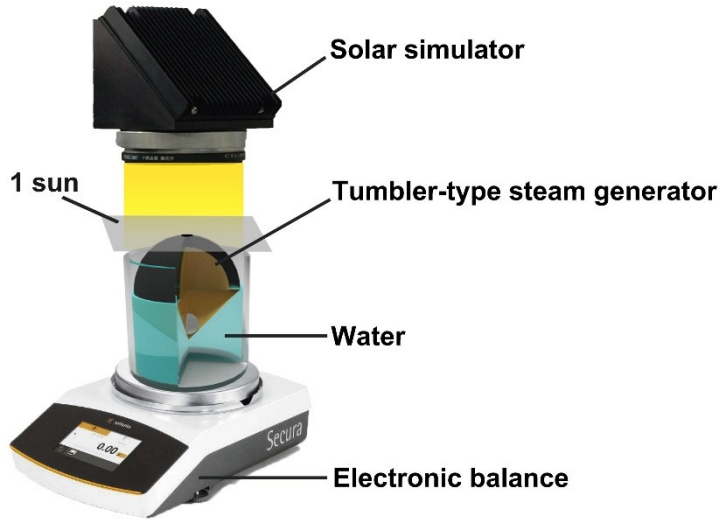


**Figure S7.** A schematic diagram of water evaporation setup.

## 9. Calculation of photothermal conversion efficiency and heat loss

(1) The photothermal conversion efficiency ($\eta$) was calculated by Equation S1[4-7],

$$\eta = \Delta m\left(L_v + Q\right)/P_{in} \qquad (S1)$$

where $\Delta m$ is the mass flux ($\Delta m = m_{Light} - m_{Dark}$) kg m$^{-2}$h$^{-1}$, $Lv$ is the latent heat of vaporization of water ($Lv$ (T)= $1.91846\times10^6[\ T/(T{-}33.91)]^2$ J kg$^{-1}$, where $T$ is the temperature of steam), $Q$ is the sensible heat of water of unit mass ($Q = c\ (T_2{-}T_1)$ J kg$^{-1}$, where $c$ is the specific heat of water, which can be assumed as a constant (4.2 J g$^{-1}$ K$^{-1}$), $T_2$ is the temperature of steam and $T_1$ is the initial temperature of the water) and $P_{in}$ is the incident solar power on the device surface.

(2) The heat loss was calculated by Equation S2-S4,[8,9]

1) Radiative loss

$$P_{rad} = \varepsilon \cdot \sigma \cdot \left(T_2^{\,4} - T_1^{\,4}\right) \qquad \text{(S2)}$$

where $\varepsilon$ is the emissivity (i.e., 0.94), $\sigma$ the Stefan–Boltzmann constant (i.e., $5.67 \times 10^{-8}$ W (m$^2$ K$^4$)$^{-1}$), $T_2$ is the temperature at the surface of the solar absorber, $T_1$ is the temperature of the adjacent environment. The radiative loss of the 3D pillared steam generator and the tumbler-shaped steam generator are calculated to be ~2.9% and ~3.4%, respectively.

2) Convective loss

$$P_{conv} = h \cdot \left(T_2 - T_1\right) \qquad \text{(S3)}$$

Where $h$ is convection heat transfer coefficient (assumed to be 5 W (m$^2$ K)$^{-1}$), $T_2$ is the temperature at the surface of the solar absorber, $T_1$ is the temperature of the adjacent environment. The convective loss of the 3D pillared steam generator and the tumbler-shaped steam generator are calculated to be ~2.2% and ~2.5%, respectively.

3) Conduction loss

$$P_{cond} = \frac{C \cdot m \cdot \Delta T}{A \cdot t} \qquad \text{(S4)}$$

Where $C$ is the specific heat capacity of water (4.2 J g$^{-1}$K$^{-1}$), $m$ is the water weights (60 g) and $\Delta T$ is increased temperature of the bulk water within 1 h, $A$ is the projected area (m$^2$), $t$ is the irradiated time (s). The conduction loss of the 3D pillared steam generator and the tumbler-type steam generator are calculated to be ~41.8% and ~5.6%, respectively.

## 10. Summary of solar evaporation performance

**Table S1**. Summary of interfacial steam generators using PAN as structural element in recent reports.

| solar absorber | floater | evaporation rate ($kg\ m^{-2}\ h^{-1}$) | type |
|---|---|---|---|
| [1]PAN/PVA/AuNR[10] | PAN/PVA/AuNR | 2.70 | direct contact |
| [2]PAN/Nylon 6/PS/CB[11] | PS | 1.24 | indirect contact |
| [3]CB/PMMA[12] | PAN | 1.30 | direct contact |
| [4]CB/PAN [13] | PVDF | 1.20 | direct contact |
| [5]Co-Zn ZIF/MoS$_2$/PAN [14] | Co-Zn ZIF/MoS$_2$/PAN | 1.39 | direct contact |
| [6]CNT/MoS$_2$/PAN [15] | CNT/MoS$_2$/PAN | 1.44 | direct contact |
| [7]RGO/cotton/PAN [16] | RGO/cotton/PAN | 1.47 | direct contact |
| [8]PAN/rGO [17] | PS | 1.46 | indirect contact |
| [9]PAN/GO [18] | PAN | 2.27 | direct contact |
| [10]SiO$_2$/MWCNTs-COOH/PAN [19] | PS | 1.28 | indirect contact |

## 11. Water evaporation in indoor and outdoor conditions
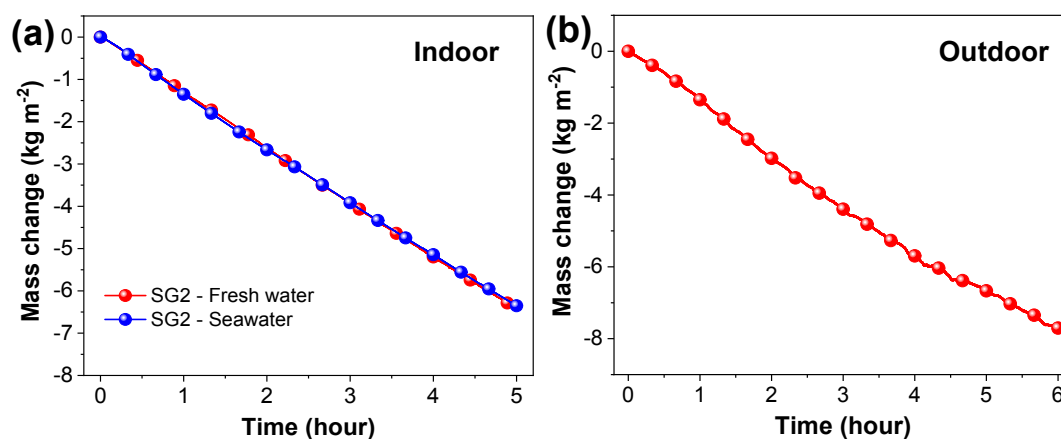


**Figure S8.** (a) Mass changes of fresh water and seawater under one sun; (b) mass change of fresh water under a real sky.

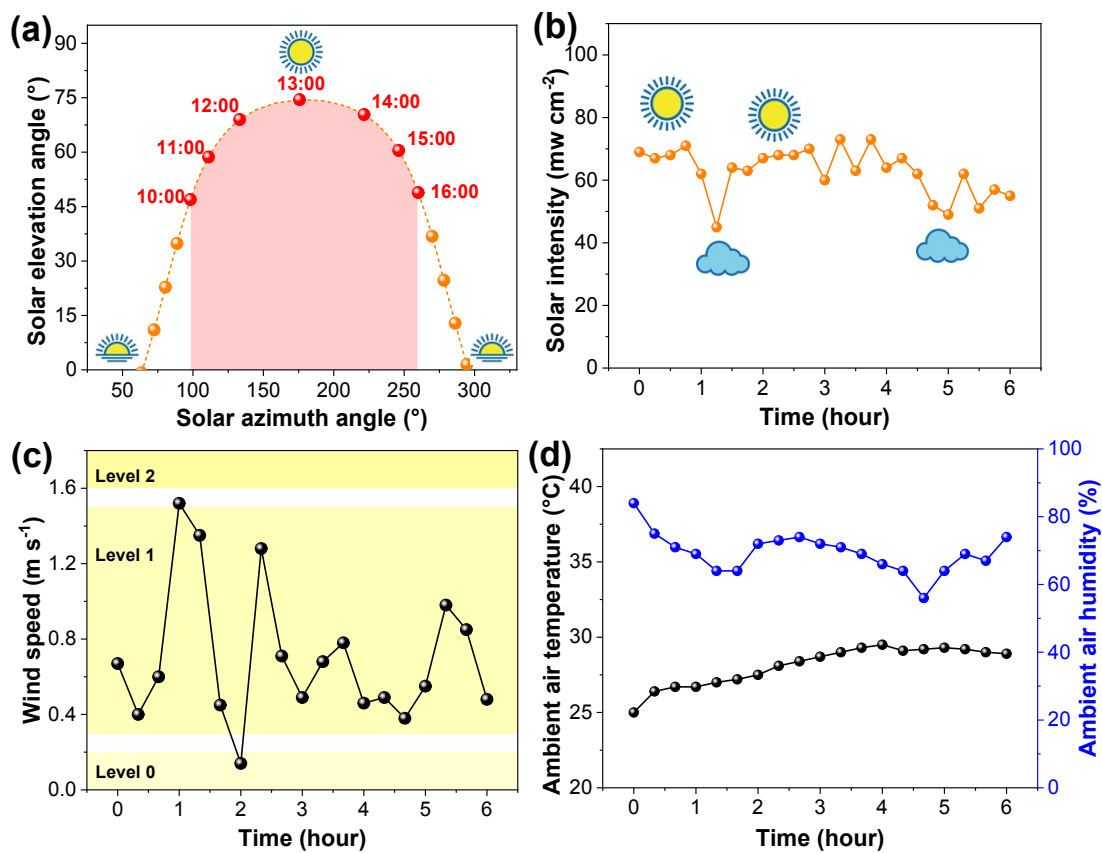## 12. Environmental parameters in outdoor measurements



**Figure S9.** (a) The Sun's position on the sky dome; (b) solar intensity, (c) air velocity and (d) ambient air temperature and humidity at outdoor measurements.
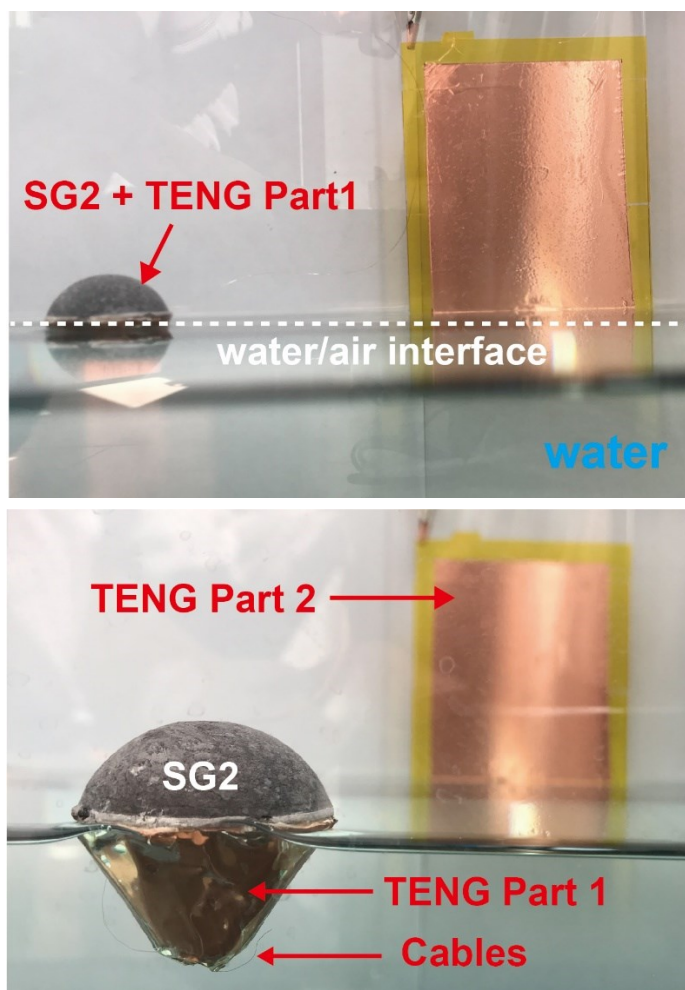
## 13. Digital photographs of the integrated system



**Figure S10.** Digital photographs of the integrated device for solar evaporation and water wave detection.
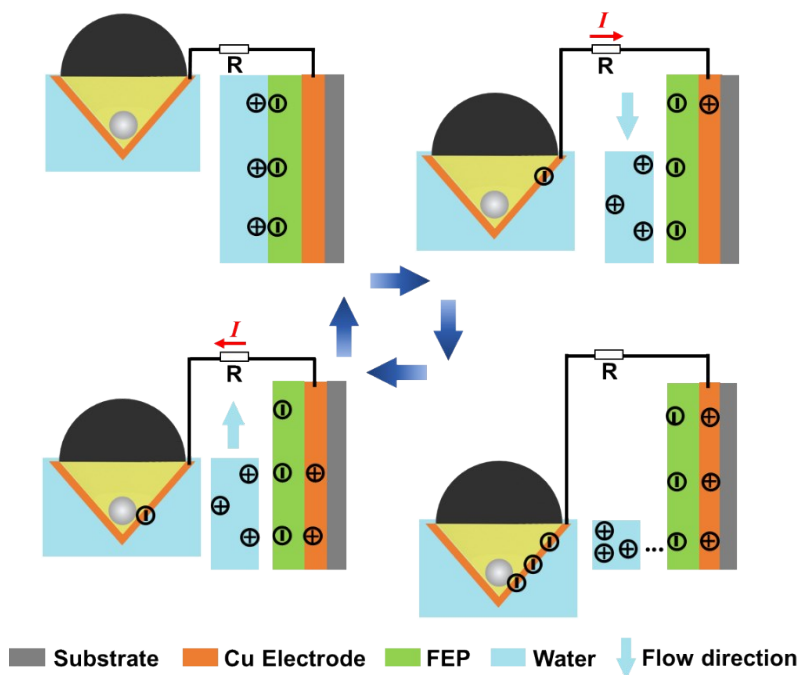
## 14. A working principle of TENG



**Figure S11.** Working principle of charge generation and transfer via liquid/solid friction.
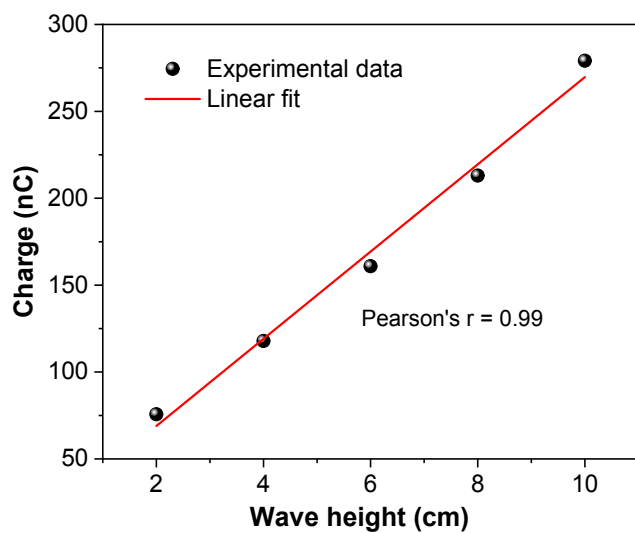
## 15. Sensitivity characterization



**Figure S12.** The Pearson correlation coefficient derived from the transferred charges and wave heights.

## 16. Calculation of wave velocity and wavelength

$$V_p(t) = S / dt \qquad \text{(S5)}$$

$$L = V_p(t) * t \qquad \text{(S6)}$$

Where $V_p$ is propagation velocity of a water wave, $S$ is the distance between TENG 2 and TENG 3, $dt$ is the interval time between two adjacent signals, and $t$ is the duration time of one signal.

## 17. References

1. W. Huang, G. Hu, C. Tian, X. Wang, J. Tu, Y. Cao and K. Zhang, *Sustainable Energy & Fuels*, 2019, **3**, 3000-3008.
2. Y. Zhang, X. Yin, B. Yu, X. Wang, Q. Guo and J. Yang, *ACS Appl. Mater. Interfaces*, 2019, **11**, 32559-32568.
3. Z. Sun, W. Li, W. Song, L. Zhang and Z. Wang, *J. Mater. Chem. A*, 2020, **8**, 349-357.
4. L. Wu, Z. Dong, Z. Cai, T. Ganapathy, N. X. Fang, C. Li, C. Yu, Y. Zhang and Y. Song, *Nat. Commun.*, 2020, **11**, 521.
5. C. Tu, W. Cai, X. Chen, X. Ouyang, H. Zhang and Z. Zhang, *Small*, 2019, **15**, 1902070.
6. C. Xing, D. Huang, S. Chen, Q. Huang, C. Zhou, Z. Peng, J. Li, X. Zhu, Y. Liu, Z. Liu, H. Chen, J. Zhao, J. Li, L. Liu, F. Cheng, D. Fan and H. Zhang, *Adv. Sci.*, 2019, **6**, 1900531.
7. X. Li, G. Ni, T. Cooper, N. Xu, J. Li, L. Zhou, X. Hu, B. Zhu, P. Yao and J. Zhu, *Joule*, 2019, **3**, 1798-1803.
8. J. Zhou, Y. Gu, P. Liu, P. Wang, L. Miao, J. Liu, A. Wei, X. Mu, J. Li and J. Zhu, *Adv. Funct. Mater.*, 2019, **29**, 1903255.
9. H. Song, Y. Liu, Z. Liu, M. H. Singer, C. Li, A. R. Cheney, D. Ji, L. Zhou, N. Zhang, X. Zeng, Z. Bei, Z. Yu, S. Jiang and Q. Gan, *Adv. Sci.*, 2018, **5**, 1800222.
10. Z. M. Huang, S. L. Li, X. Cui, Y. P. Wan, Y. F. Xiao, S. Tian, H. Wang, X. Z. Li, Q. Zhao and C. S. Lee, *J. Mater. Chem. A*, 2020, **8**, 10742-10746.
11. Y. Jin, J. Chang, Y. Shi, L. Shi, S. Hong and P. Wang, *J. Mater. Chem. A*, 2018, **6**, 7942-7949.
12. W. C. Xu, X. Z. Hu, S. D. Zhuang, Y. X. Wang, X. Q. Li, L. Zhou, S. N. Zhu and J. Zhu, *Adv. Energy Mater.*, 2018, **8**, 1702884.
13. T. T. Gao, Y. J. Li, C. J. Chen, Z. Yang, Y. D. Kuang, C. Jia, J. W. Song, E. M. Hitz, B. Y. Liu, H. Huang, J. Y. Yu, B. Yang and L. B. Hu, *Small Methods*, 2019, **3**, 1800176.
14. H. Peng, L. Zhang, M. Li, M. Liu, C. Wang, D. Wang and S. Fu, *Chem. Eng. J.*, 2020, **397**, 125410.
15. B. Zhu, H. Kou, Z. Liu, Z. Wang, D. K. Macharia, M. Zhu, B. Wu, X. Liu and Z. Chen, *ACS Appl. Mater. Interfaces*, 2019, **11**, 35005-35014.
16. Q. Zhang, H. J. Yang, X. F. Xiao, H. Wang, L. Yan, Z. X. Shi, Y. L. Chen, W. L. Xu and X. B. Wang, *J. Mater. Chem. A*, 2019, **7**, 14620-14628.
17. X. Fan, B. Lv, Y. Xu, H. Huang, Y. Yang, Y. Wang, J. Xiao and C. Song, *Solar Energy*, 2020, **209**, 325-333.
18. L. Wang, C. Liu, H. Wang, Y. Xu, S. Ma, Y. Zhuang, W. Xu, W. Cui and H. Yang, *ACS*

*Appl. Mater. Interfaces*, 2020, **12**, 24328-24338.

19. Q. B. Qi, W. Wang, Y. Wang and D. Yu, *Sep Purif Technol*, 2020, **239**, 116595.